Observer Design for Particle Size Distribution in Emulsion Polymerization

David Edouard, Nida Sheibat-Othman, and Hassan Hammouri
Laboratoire d'Automatique et de Génie des Procédés (LAGEP), University Lyon I, Bāt 308, 69622 Villeurbanne Cedex, France

DOI 10.1002/aic.10559
Published online September 13, 2005 in Wiley InterScience (www.interscience.wiley.com).

Monitoring of the particle size distribution (PSD) in emulsion polymerization is a very important task to improve the product quality. However, on-line sensors used to measure PSD, such as capillary hydrodynamic fractionation, usually require taking samples and the analysis time is still too long for control. This work proposes the combination of mathematical models with existing on-line sensors to obtain a continuous estimation of the PSD by constructing nonlinear estimators. Simulations of the observers show that they are able to detect particle nucleation and to give an estimation of the whole PSD. © 2005 American Institute of Chemical Engineers *AIChE J,* 51: 3167–3185, 2005
Keywords: emulsion polymerization, particle size distribution, observer, estimation, modeling, monitoring

Introduction

Controlling the particle size distribution (PSD) is an important task in emulsion polymerization processing. The PSD is an important parameter that affects the polymer rheology, adhesion, optical properties, mechanical strength, and the latex stability and is an important parameter in control of process productivity because it determines the reaction rate. The particle size is also an important parameter for film formation (see, for example, Geurts et al.[1]). In addition, by producing multimodal latices, Guyot et al.[2] were able to maximize the latex solids content and to reduce its viscosity.

One of the difficulties in controlling the PSD lies in the lack of on-line instruments that are able to measure it continuously and on-line. Quasi-elastic light scattering (QELS) is usually used to measure the particle size for monomodal latices. On-line spectroscopic techniques such as near-infrared or Raman spectroscopies have also been used to measure the particle size in polymerization processes.[3] However, with respect to light-scattering techniques, the QELS technique is more efficient for monomodal latices. Multimodal latices can be measured by off-line microscopic techniques, transmission electron microscopy (TEM), or scanning electron microscopy (SEM), all of which require sample preparation. A disc centrifuge photosedimentometer is also used off-line to measure the PSD of multimodal latices with a wide range of diameters. For on-line measuring the PSD of multimodal latices, separation techniques such as capillary hydrodynamic fractionation (CHDF)[4] and flow-field flow fractionation (f-FFF)[5,6] give good performances. In CHDF, the particle size is obtained from the elution time by calibration. The relative particle concentration is obtained by UV absorbance. In f-FFF, usually multiangle laser light scattering is used as a detector, which allows absolute determination of the particle size. In CHDF, small particles are retained in the column for a longer time and thus larger particles exit first, whereas in f-FFF smaller particles are the first to leave the column. Sample analysis takes about 12 min in CHDF and a waiting period of 10 min is required between the samples. In f-FFF, the separation phase takes 20–30 min.

Another factor retarding the development of PSD control lies in the difficulty in modeling and determining the kinetic parameters of the system. Gilbert[7] proposed the 0–1 model and identified the kinetics for styrene polymerization. This model was then used by Coen et al.[8] to model coagulation and secondary nucleation. Using the same model, Sood[9] used CHDF and calorimetry to study the influence of the monomer addition protocol, emulsifier, and initiator charges on the evolution of the PSD of a seeded styrene system.

Correspondence concerning this article should be addressed to N. Sheibat-Othman at nida.othman@lagep.univ-lyon1.fr.

Immanuel et al.[10] used the pseudo-homopolymerization model, initially proposed by Storti et al.,[11] to study the PSD for vinyl acetate and butyl acrylate polymerizaion and in a later work[4] to study particularly the effect of surfactant type and coagulation on the PSD using CHDF and densimetry. This model was also used by Ginsburger et al.[12] to model and identify styrene/butyl acrylate copolymerization.

The difficulties in controlling the PSD also arise from the fact that the PSD is represented by partial differential equations that can be solved by different approximation methods (discretization methods, method of moments). Ramkrishna[13] gave a good presentation of the population balance equations and the mathematical methods that can be used to solve them. Immanuel and Doyle[14] presented an efficient solution technique for population balance equations that is not based on approximating the population balance equations.

Finally, applying techniques of estimation and control to these models requires theoretical validation. Semino and Ray[15,16] proposed a theoretical study of the controllability of the PSD of continuous-emulsion polymerization reactors. The theoretical controllability of the system was demonstrated using a linearized process model and validated by simulation to the nonlinear model. The authors showed that the PSD is controllable using the manipulating variables: surfactant, initiator and inhibitor concentrations, and assuming monomer conversion and total number of particles in the reactor to be measured. However, the authors outline that the process is easier to be controlled using the surfactant flow rate that acts directly on the concentration of micelles. An experimental study of the evolution of the PSD in continuous reactors was done by Ohmura et al.[17]

Because of these difficulties, only few papers in the literature have treated controlling the whole PSD. Crowley et al.[18] used the 0–1 model to obtain a bimodal target distribution of styrene polymerization. The authors compared both the surfactant feed rate and free concentration as control variables that were calculated by an optimization algorithm. To control the PSD, Zeaiter et al.[19] used the 0–1 model for styrene polymerization. The authors applied an optimal control strategy that calculates on-line the desired monomer flow rate required to obtain the desired PSD. Immanuel and Doyle[20] proposed an open-loop control strategy to control the PSD for vinyl acetate and butyl acrylate polymerization. The generated algorithm was based on the optimization of profiles of the feed rate of monomer and surfactant to obtain a target PSD. Later on, Immanuel and Doyle[21] controlled the PSD using a multiobjective optimization algorithm by both open-loop and feedback algorithms. Doyle et al.[22] developed a hybrid model–based approach to control the PSD of styrene polymerization. The algorithm uses the partial least-square model to optimize the feed rates of surfactant and initiator.

Using estimators in the control algorithm is interesting to obtain information about the nonmeasured properties and to overcome modeling errors. Actually, because the model is used in a closed-loop manner by using the process outputs, this allows detection of process mismodeling. In this study, we propose estimators of the PSD and the nucleation rate. The estimators are developed based on a new model derived from the 0–1 model. After a presentation of the 0–1 model, the new model is developed, validated, and compared to the original 0–1 model. Then estimators of the PSD and nucleation rate are constructed using this model.

Modeling

Population balance equations

The general population balance equation is given by the following hyperbolic differential equation:

$$\frac{\partial \zeta(\eta, t)}{\partial t} + \frac{\partial \left[\zeta(\eta, t) \dfrac{d\eta}{dt} \right]}{\partial \eta} = \Re_{generation}(\eta, t) \qquad (1)$$

where $\zeta(\eta, t)$ is the population density function, $\Re_{generation}$ is the rate of generation of new members in the population, and $d\eta/dt$ accounts for variation in the property η with time.

In emulsion polymerization, the PSD can be described by two types of models. Both models couple the population balance equations and the reaction kinetics in the aqueous phase and in the polymer particles: initiation, propagation, terminations, transfer, nucleation, growth, and coagulation. The first model is the pseudobulk model that is available for large particles in which more than one free radical can coexist for a significant period. To represent these kinetics, two differential equations are necessary. The first equation represents the evolution of the PSD for particles that have zero, one, or more radicals and the second equation represents the number of radicals in those particles as follows (for more details see Immanuel et al.[10]):

$$\begin{cases} \dfrac{\partial n(r, t)}{\partial t} + \dfrac{\partial [n(r, t)G(r)]}{\partial r} = \Re_{nuc}\delta(r - r_{nuc}) + \Re_{coagulation} \\ \dfrac{\partial \bar{n}(r, t)}{\partial t} = \acute{\Re}_{entry} - \acute{\Re}_{desorption} - 2\acute{\Re}_{termination} \end{cases} \qquad (2)$$

The particle density $n(r, t)dr$ is defined as the number of moles of particles of size between r and $r + \delta r$ at time t; $\Re_{nuc}$ is the rate of nucleation; $\delta(r - r_{nuc})$ is the Dirac delta function, which is unity at $r = r_{nuc}$ and zero elsewhere; $G(r)$ is the particle growth [$G(r) = dr/dt$]; and $\acute{\Re}_{entry}$, $\acute{\Re}_{desorption}$, and $\acute{\Re}_{termination}$ are the total rates of entry, desorption, and termination within a single particle of size between r and $r + \delta r$, respectively.

The second model is the zero–one model.[7] This model is adapted only for systems with the number of radicals per particle equal to 0 or 1. Therefore, this model is generally available for small particles, except for monomers that propagate rapidly, such as acrylates, where small particles exhibit pseudobulk kinetics.[23] This model distinguishes particles that have a polymeric radical (n_{1p}), particles that have no radicals (n_0), and particles that have a monomeric radical (n_{1m}), as shown in Figure 1 Nucleation produces particles with one radical (n_{1p}). A particle of type (n_{1p}) becomes a particle of category n_0 if a new radical enters in or becomes a particle of the category n_{1m} if the radical it contains becomes a monomeric radical by transfer to monomer or small chains. The distinction

between particles containing one radical and particles containing a monomeric radical is necessary in the 0–1 model because desorption concerns only monomeric radicals.

Because the objective of this work is to monitor the PSD starting from the beginning of the reaction, where the particles are small, the 0–1 model will be used throughout this work to monitor the process. The particles were assumed to be colloidally stable, and therefore coagulation is not represented but can, however, be added to the 0–1 model. (For more details on the model see Crowley et al.[18])

$$\begin{cases} \dfrac{\partial n_0(r,\,t)}{\partial t} = \rho(r,\,t)[n_{1p}(r,\,t) + n_{1m}(r,\,t) - n_0(r,\,t)] + k_{des}(r)n_{1m}(r,\,t) \\ \dfrac{\partial n_{1p}(r,\,t)}{\partial t} = \rho_{ent-r}(r,\,t)n_0(r,\,t) - [\rho r,\,t) + k_{tr}[M]_P]n_{1p}(r,\,t) + k_{pe}[M]_P n_{1m}(r,\,t) - \dfrac{\partial[G(r)n_{1p}(r,\,t)]}{\partial r} + \Re_{nuc}\delta(r - r_{nuc}) \\ \dfrac{\partial n_{1m}(r,\,t)}{\partial t} = \rho_{ent-m}(r,\,t)n_0(r,\,t) + k_{tr}[M]_P n_{1p}(r,\,t) - n_{1m}(r,\,t)[\rho(r,\,t) + k_{pe}[M]_P + k_{des}(r)] \end{cases} \quad (3)$$

where $\rho_{ent-r}(r,\,t)$ represents the rate of entry of a radical of length i ($z \le i \le j_{\text{crit}-1}$) into particles; $\rho_{ent-m}(r,\,t)$ represents the rate of entry of a monomeric radical into particles; and $\rho(r,\,t) = \rho_{ent-r}(r,\,t) + \rho_{ent-m}(r,\,t)$ is the overall rate of radical entry into particles.

The total number of particles of size between r and $r + dr$ is given by

$$n(r,\,t) = n_0(r,\,t) + n_{1p}(r,\,t) + n_{1m}(r,\,t) \quad (4)$$

Micellar ($\Re_{nuc-mic}$) and homogeneous ($\Re_{nuc-hom}$) nucleations cause formation of very small particles containing a radical. The total nucleation rate ($\Re_{nuc} = \Re_{nuc-hom} + \Re_{nuc-mic}$) thus acts as a boundary condition of Eq. 3. This results in a Dirichlet condition as follows:

$$n_{1p}(r_{nuc},\,t) = \frac{\Re_{nuc}(t)}{G(r_{nuc})} \quad (5)$$

with

$$\begin{cases} \Re_{nuc-mic} = \displaystyle\sum_{i=z}^{j_{crit}-1} k_{em,i}[Micelle][IM_i]V^{aq} \\ \Re_{nuc-hom}(t) = k^{aq}_{p,(j_{crit}-1)}[M]_{aq}[IM_{j_{crit}-1}]V^{aq} \end{cases} \quad (6)$$

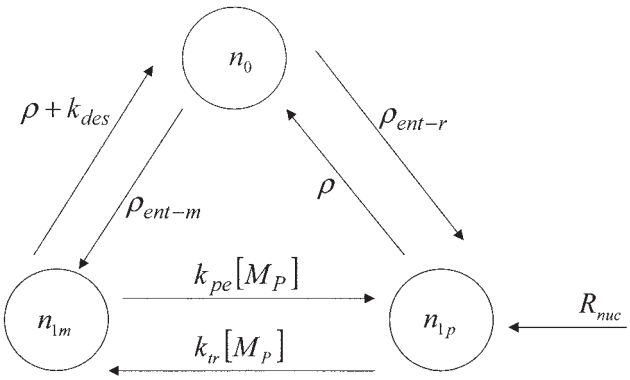

Figure 1. 0–1 model.

The average number of radicals in particles of size r at time t [$\bar{n}(r,\,t)$] is the ratio of particles containing either a radical or a monomeric radical to the total number of particles, which theoretically cannot exceed 1:

$$\bar{n}(r,\,t) = \frac{n_{1p}(r,\,t) + n_{1m}(r,\,t)}{n(r,\,t)} \quad (7)$$

Aqueous-phase reactions

Particle nucleation and radical entry/exit from the particles depend on the concentration of micelles and radicals in the aqueous phase. Therefore, to solve the population balance equations, material balances in the aqueous phase should be studied.

The polymerization process starts by the initiator decomposition (I) in the aqueous phase producing primary radicals ($I^{\bullet}$) that react with monomer molecules (M) to generate oligomeric radicals (IM_i). The main reactions taking place in the aqueous phase are illustrated in Table 1.

Radical entry and desorption from particles is governed by the coefficients (k_{eE}, $k_{e,i}$, and k_{des}) that are assumed to be diffusion controlled (D_w) and depend on the particle radius as shown in Table 2. [E] is the concentration of monomeric radicals that have a lipophilic nature and can therefore diffuse easily into particles and desorb out of them. [T] is the total concentration of radicals in the aqueous phase, defined by

$$[T] = \sum_{i=1}^{j_{crit}-1} [IM_i] + [E] + [I^{\bullet}]$$

where z is the critical chain length at which polymer radicals can enter polymer particles or micelles (micellar nucleation) and j_{crit} is the chain length at which the radicals become insoluble in water and thus precipitate as new particles (homogeneous nucleation).

Writing the material balances of the species in the aqueous phase requires the integration of the whole PSD:

$$\frac{1}{V^{aq}}\frac{d([I]V^{aq})}{dt} = \frac{Q_I}{V^{aq}} - k_d[I] \quad (8)$$

Table 1. Aqueous-Phase Reactions

Primary radical initiation	$I \xrightarrow{k_d} 2I^{\cdot}$
Polymer radical initiation	$I^{\cdot} + M \xrightarrow{k_{pI}^{aq}} IM_1$
Propagation	$IM_i + M \xrightarrow{k_{pi}^{aq}} IM_{i+1}$
Termination	$\begin{cases} IM_i + T \\ I^{\cdot} + T \xrightarrow{k_t^{aq}} \text{inactive polymer chain} \\ E + T \end{cases}$
Radical transfer to monomer	$IM_i + M \xrightarrow{k_{tr}^{aq}} E + \text{inactive polymer chain}$
Micellar nucleation	$IM_i + Micelle \xrightarrow{k_{em,i}} \text{new particle}\ (z \le i \le j_{crit} - 1)$
Homogeneous nucleation	$IM_{j_{crit}-1} + M \xrightarrow{k_{pj_{crit}-1}^{aq}} \text{new particle}$
Radical entry into particle	$IM_i + particle_n \xrightarrow{k_{e,i}} particle_{n+1}$
Entry of a monomeric radical into particles	$E + particle_n \xrightarrow{k_{eE}} particle_{n+1}$

$$\frac{1}{V^{aq}}\frac{(d[I^{\cdot}]V^{aq})}{dt} = 2k_d[I] - (k_{pI}^{aq}[M]_{aq} + k_t^{aq}[T])[I^{\cdot}] \quad (9)$$

$$\frac{1}{V^{aq}}\frac{d([IM_1]V^{aq})}{dt} = k_{pI}^{aq}[M]_{aq}[I^{\cdot}] - (k_{p,1}^{aq}[M]_{aq} + k_t^{aq}[T] + k_{tr}^{aq}[M]_{aq})[IM_1] \quad (10)$$

$$\frac{1}{V^{aq}}\frac{d\{[IM_i]V^{aq}(t)\}}{dt} = k_{p,i-1}^{aq}[M]_{aq}[IM_{i-1}] - (k_{p,i}^{aq}[M]_{aq} + k_t^{aq}[T] + k_{tr}^{aq}[M]_{aq})[IM_i],\ i = 2,\ z-1 \quad (11)$$

Table 2. Description of Parameters

Parameter	Description
$G(r)$	$\frac{k_p[M]_P MW_m}{4\pi r^2 d_p N_A}$
k_{des}	$\frac{3D_w[M]_{aq}^{sat}}{r_s^2[M]_P^{sat}}$
$k_{e,i}$	$r_s\left(\frac{4\pi NaD_w}{\sqrt{i}}\right) \quad (z \le i \le j_{crit} - 1)$
k_{eE}	$4\pi r_s NaD_w$
$k_{em,i}$	$r_{mic}\left(\frac{4\pi NaD_w}{\sqrt{i}}\right) \quad (z \le i \le j_{crit} - 1)$
r_s	$r\left(\frac{d_m}{d_m - [M]_P^{sat} MW_m}\right)^{1/3}$

$$\frac{1}{V^{aq}}\frac{d\{[IM_i]V^{aq}(t)\}}{dt} = k_{p,i-1}^{aq}[M]_{aq}[IM_{i-1}] - (k_{p,i}^{aq}[M]_{aq} + k_t^{aq}[T] + k_{tr}^{aq}[M]_{aq} + k_{em,i}[Micelle])[IM_i] - \frac{1}{V^{aq}}\int_{r_{nuc}}^{\infty} k_{e,i}n(r)dr[IM_i] \qquad i = z,\ j_{crit} - 1 \quad (12)$$

$$\frac{1}{V^{aq}}\frac{d\{[E]V^{aq}(t)\}}{dt} = \frac{1}{V^{aq}}\int_{r_{nuc}}^{\infty} k_{des}(r)n_{1m}(r)dr + k_{tr}^{aq}[M]_{aq}[T] - \frac{1}{V^{aq}}\int_{r_{nuc}}^{\infty} k_{eE}(r)[E]n(r)dr - k_t^{aq}[E][T] \quad (13)$$

where V^{aq} is the volume of the aqueous phase, Q_I is the initiator flow rate (mol/s), and $[I]$ is the initiator concentration (mol/dm^3).

It is important to note that species in the aqueous phase are difficult to measure precisely. Therefore, determination of the kinetics of a system is not easy. Moreover, these species are usually affected by the inhibition phenomena. Therefore, attention should be made when using these equations in an open-loop algorithm.

Monomer material balance and partitioning between the phases

The amount of residual monomer can be calculated either by doing a balance on the monomer, taking into account the reaction rate,

$$\frac{dN_m(t)}{dt} = Q_m - \underbrace{k_p \mu [M]_P}_{Rp(t)} \tag{14}$$

or by doing a mass balance on the polymer ($[M]_P$),

$$\begin{cases} m_p(t) = \dfrac{4}{3}\,\pi d_p N_A \displaystyle\int_{r_{nuc}}^{\infty} r^3 n(r) dr \\ N_m(t) = N_m^T(t) - \dfrac{m_P(t)}{MW_m} \end{cases} \tag{15}$$

where $N_m(t)$ and $N_m^T(t)$ are the number of moles of residual monomer and the total number of moles of monomer introduced to the reactor at time t, respectively; Q_m is the monomer flow rate (mol/s); m_P is the polymer mass; and N_A is Avogadro's number. Both ways require the integration of the PSD because μ, the number of moles of radicals in the polymer particles, depends on the average number of radicals in the polymer particles of any size at time t [$\bar{n}(t)$] and the total number of particles in the reactor (N_P^T):

$$\mu = \frac{\bar{n}(t) \times N_P^T(t)}{N_A} \tag{16}$$

where N_P^T can be obtained by integrating the function representing the PSD [$n(r, t)$] over r:

$$N_P^T(t) = \int_{r_{nuc}}^{\infty} n(r, t)\, N_A dr \tag{17}$$

and $\bar{n}(t)$ can be related to $\bar{n}(r, t)$ using Eq. 7, which gives the following:

$$\bar{n}(t) = \frac{\displaystyle\int_{r_{nuc}}^{\infty} \bar{n}(r, t) n(r, t) dr}{\displaystyle\int_{r_{nuc}}^{\infty} n(r, t) dr} \tag{18}$$

During interval II (saturation of polymer particles), the concentration of monomer in the polymer particles {$[M]_P^{sat}$ (mol/dm^3)} is calculated using the partitioning coefficients[18]:

$$[M]_{aq}^{sat} = \frac{d_m}{K_{d-aq} MW_m}$$

where $[M]_{aq}^{sat}$ is the concentration of monomer in the aqueous phase under saturation (mol/dm^3):

$$[M]_P^{sat} = [M]_{aq}^{sat} \times K_{p-aq}$$

Because the 0–1 model—used during this entire study—is adapted to small particles in the absence of gel effect (therefore, it is rarely available during interval III), we intended to maintain the polymer particles under saturation in all the simulations ($[M]_P = [M_P^{sat}]$). Therefore, the model representing the concentration of monomer in the polymer particles in interval III is not necessary.

Surfactant material balances and micelle concentration

The surfactant is assumed to be introduced at a flow rate Q_S (mol/s) that is smoothed by a first-order model of reference:

$$\frac{dN_S(t)}{dt} = Q_S(t) \tag{19}$$

where N_S is the total number of moles of surfactant in the reactor.

The concentration of free surfactant in the aqueous phase ($[S^{aq}]$) can be calculated from the following balance equation:

$$\underbrace{[S^{aq}]V^{aq}}_{N_S^{aq}} = N_S - N_S^P - N_S^d$$

where N_S^P and N_S^d are the number of moles of surfactant adsorbed on the surface of particles and droplets as given by the following thermodynamic relationships:

$$N_S^d = \frac{3V^d}{a_{sd} r_d N_A} \tag{20}$$

$$N_S^P = \frac{S_{par} b_s [S^{aq}]}{a_{sp} N_A (1 + b_s [S^{aq}])} \tag{21}$$

where S_{par} is the total particle surface:

$$S_{par} = 4\pi N_A \int_{r_{nuc}}^{\infty} n(r) r^2 dr \tag{22}$$

and V^d is the droplets volume (dm^3).

The concentration of micelles ($[Micelle]$) is then calculated using the following expression:

$$[Micelle] = \max\left(0, \frac{[S^{aq}] - CMC}{n_{agg}}\right) \tag{23}$$

where CMC is the critical micelle concentration and n_{agg} is the aggregation number for the surfactant. This signifies that micelles exit only if the concentration of surfactant in the reactor exceeds the CMC. Particle nucleation occurs at a minimum size (r_{nuc}) as a result of the presence of micelles that are formed under sufficient concentration of surfactant. The rate coefficient of particle nucleation ($k_{em,i}$) is diffusion controlled and calculated using the radius of micelles (r_{mic}) (Table 2).

Mathematical Treatment

Experimental measurement of the PSD, by CHDF for example, gives the total number of particles of size r [$n(r)$] and does not give $n_{1p}(r)$, $n_{1m}(r)$, and $n_0(r)$ individually. Therefore, constructing an estimator using this measurement would be easier

using a model that gives $n(r)$ directly rather than using the 0–1 model that describes the three states individually. Therefore, developing a model for small particles that have the same form as the pseudobulk model would be of interest.

For this reason, the 0–1 model presented above is used in this section to develop a new model that has the form of the pseudobulk model.

Development of a bulk-like model for the 0–1 system

The new model is developed using equation system 3. The change of variables to obtain the new model consists of the equation of $\bar{n}(r, t)$ (Eq. 7) that can be written under the following form:

$$\bar{n}(r, t) = \frac{N(r, t)}{n(r, t)} \tag{24}$$

with $N(r, t) = n_{1p}(r, t) + n_{1m}(r, t)$.

The sum of the three equations in the 0–1 model (Eq. 3) gives a balance on the total number of particles in the reactor $[n(r, t)]$:

$$\frac{\partial n(r, t)}{\partial t} = -\frac{\partial G(r) n_{1p}(r, t)}{\partial r} + \Re_{nuc}\delta(r - r_{nuc}) \tag{25}$$

In this model, the particles n_{1m} are assumed not to be growing, that is,

$$\frac{\partial G(r) n_{1m}(r, t)}{\partial r} = 0$$

This is explained by the fact that the lapse of time during which a particle is of type n_{1m} is very small. Actually a particle of type n_{1m} becomes very quickly either an n_{1p} (if the monomeric radical propagates), in which case it grows normally, or becomes an n_0 (if the monomeric radical desorbs or terminates), in which case it does not grow. For this reason, assuming that the particles (n_{1m}) grow as the particles of type n_{1p} does not affect the evolution of the PSD. In this case, Eq. 25 can be written under the following form:

$$\frac{\partial n(r, t)}{\partial t} = -\frac{\partial G(r)[n_{1p}(r, t) + n_{1m}(r, t)]}{\partial t} + \Re_{nuc}\delta(r - r_{nuc}) \tag{26}$$

By combining Eqs. 24 and 25 with the approximation given by Eq. 26, the following model is obtained for $n(r, t)$:

$$\frac{\partial n(r, t)}{\partial t} = -\frac{\partial G(r)\bar{n}(r, t)n(r, t)}{\partial r} + \Re_{nuc}\delta(r - r_{nuc}) \tag{27}$$

and the following equation can be obtained for $\bar{n}(r, t)$ by deriving Eq. 24 with respect to time:

$$\frac{\partial \bar{n}(r, t)}{\partial t} = \frac{n(r, t)\dfrac{\partial N(r, t)}{\partial t} - N(r, t)\dfrac{\partial n(r, t)}{\partial t}}{n^2(r, t)} \tag{28}$$

In a similar way, by combining Eqs. 3, 24, 26, and 28, the following equation can be derived:

$$\frac{\partial \bar{n}(r, t)}{\partial t} = \rho(r, t)[1 - 2\bar{n}(r, t)] + \frac{\partial[G(r)\bar{n}(r, t)n(r, t)]}{\partial r}\left[\frac{\bar{n}(r, t) - 1}{n(r, t)}\right] - \frac{k_{des}(r)n_{1m}(r, t)}{n(r, t)} \tag{29}$$

Applying the quasi-steady-state assumption for $[n_{1m}(r, t)]$, as suggested by Crowley et al.,[18] the following algebraic equation is obtained from Eq. 3:

$$n_{1m}(r, t) = \frac{\rho_{ent-m}(r, t)n_0(r, t) + k_{tr}[M]_P n_{1p}(r, t)}{\rho(r, t) + k_{pe}[M]_P + k_{des}(r)}$$

Using the definitions of $N(r, t)$, $n(r, t)$, and Eq. 24, the expression of $n_{1m}(r, t)$ can be rewritten under the following form:

$$n_{1m}(r, t) = \frac{\rho_{ent-m}(r, t)n(r, t)[1 - \bar{n}(r, t)]}{\rho(r, t) + [M]_P(k_{pe} + k_{tr}) + k_{des}(r)} + \frac{k_{tr}[M]_P\bar{n}(r, t)n(r, t)}{\rho(r, t) + [M]_P(k_{pe} + k_{tr}) + k_{des}(r)} \tag{30}$$

Finally, the new model (bulk-like model) representing the PSD of a 0–1 system is therefore the following:

$$\begin{cases} \text{(a)} \quad \dfrac{\partial n(r, t)}{\partial t} = -\dfrac{\partial[G(r)\bar{n}(r, t)n(r, t)]}{\partial r} + \Re_{nuc}\delta(r - r_{nuc}) \\ \text{(b)} \quad \dfrac{\partial \bar{n}(r, t)}{\partial t} = \rho(r, t)[1 - 2\bar{n}(r, t)] + \dfrac{\partial[G(r)\bar{n}(r, t)n(r, t)]}{\partial r}\left[\dfrac{\bar{n}(r, t) - 1}{n(r, t)}\right] \\ \quad + k_{des}(r)\left\{\dfrac{\rho_{ent-m}(r, t)[\bar{n}(r, t) - 1]}{\rho(r, t) + [M]_P(k_{pe} + k_{tr}) + k_{des}(r)} - \dfrac{k_{tr}[M]_P\bar{n}(r, t)}{\rho(r, t) + [M]_P(k_{pe} + k_{tr}) + k_{des}(r)}\right\} \end{cases} \tag{31}$$

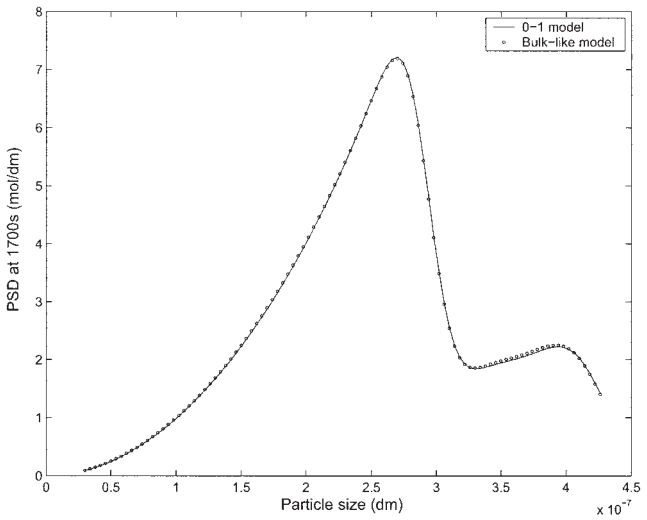

Figure 2. PSD at 1700 s (without desorption).

with the following boundary conditions:

$$n(r_{nuc}, t) = \frac{\Re_{nuc}(t)}{G(r_{nuc})} \qquad \text{and} \qquad \bar{n}(r_{nuc}, t) = 1$$

As in the 0–1 model or even in the pseudobulk model, $\bar{n}(r, t)$ has no meaning if $n(r, t) = 0$, that is, if there are no particles of size r at time t. Actually, the equation that allows us to calculate $\bar{n}(r, t)$ in the 0–1 model is singular if $n(r, t) = 0$ (Eq. 7). This singularity is maintained in the new representation of the 0–1 model derived above (bulk-like model). Therefore, a test has to be done on the value of the PSD before calculating $\bar{n}(r, t)$. If $n(r, t) = 0$, then $\bar{n}(r, t)$ is not calculated, or taken to be zero.

Numerical solution

The population balance equations for the 0–1 system given by Eq. 3 and the bulk-like model (Eq. 31) are solved by the finite-difference method of order 1 applied on the derivative with respect to r (particle radius). This approximates the integro-partial differential equations by ordinary differential equations with respect to time and discrete radius increment. An equal increment of radius is used ($\delta r = 0.4$ nm). So, a large but manageable number of coupled ordinary equations is obtained.

The finite-difference method is one of the discretization techniques applied to solve the population balance equations that is easy to use. However, approximating the derivatives using this method might result in erroneous oscillations in the distribution. In this work, no effort was made to improve the approximation method. The finite-element method was found to be sufficient to compare the two models and to test the observers' robustness. It remains yet important to develop more robust techniques to solve the population balance equations under hard conditions.

The parameters used for simulation correspond to those of styrene polymerization at 50°C that could be found in the literature.

Comparisons between the original and bulk-like models for the 0–1 system

The bulk-like model still describes the PSD of a 0–1 system. The equation of $\bar{n}(r, t)$ contains the terms related to absorption/desorption and transfer that are dispersed between the equations of the 0–1 model. To calculate $\bar{n}(r, t)$, the PSD has to be known and integrated as in the 0–1 model.

The main reason that encouraged us to write the model under this form is the facility of applying the observers, as will be seen in the next section. This is because the state of the system $[n(r, t)]$ is the direct measurement and property we are interested in controlling. A second advantage of this form is that the bulk-like model allows us to study easily the influence of each parameter on $\bar{n}(r, t)$ and therefore on $n(r, t)$. For instance, if desorption or transfer is neglected, then only the equation of $\bar{n}(r, t)$ is modified and the equation of $n(r, t)$ is maintained without any change.

Finally, the bulk-like model simplifies the transition between small and large particles. Actually, to calculate the PSD of small particles, the bulk-like model will be used and then, for large particles, the pseudobulk model can be applied. This will require changing the equation of $\bar{n}(r, t)$ only for large particles, whereas the same equation of $n(r, t)$ continues to represent the PSD. When the 0–1 model is used to describe the PSD of small particles, the transition to large particles represented by the pseudobulk model that is completely different from the 0–1 model would be difficult.[23]

To validate the bulk-like model, it was compared to the 0–1 model by simulation under the same conditions. Two cases seemed of interest to be studied: In the first case, no desorption is assumed $[k_{des}(r) = 0]$ and in the second case, the desorption is calculated using the equation represented in Table 2.

Figures 2–5 represent the PSD and $\bar{n}(r, t)$ without and with desorption, respectively. The figures show that the bulk-like model gives very similar results as the 0–1 model. It can also be seen that when no desorption takes place $\bar{n}(r, t)$ is equal to 1 for most particle sizes, which is the maximum allowable value in this model. However, when desorption takes place, $\bar{n}(r, t)$ has smaller values and increases with the particle size.

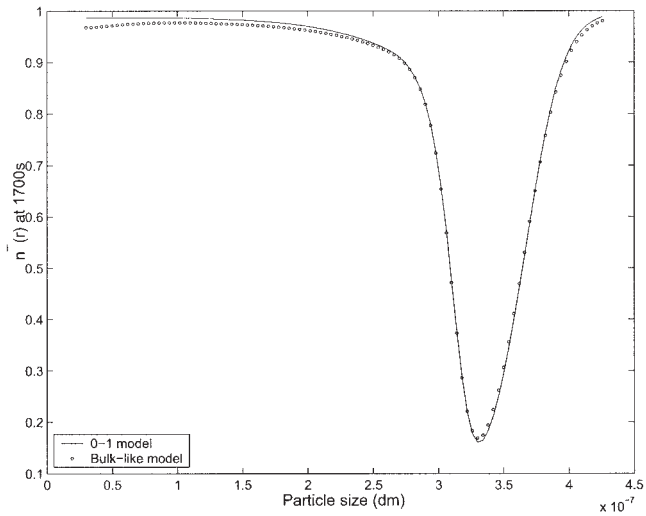

Figure 3. Average number of radicals per particle at 1700 s (without desorption).

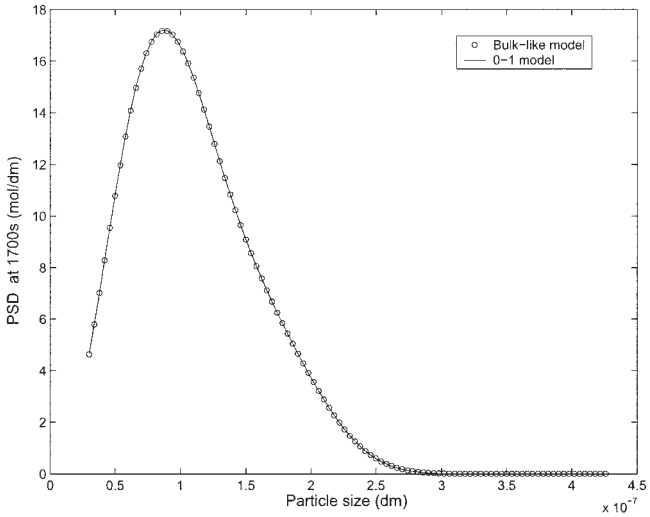

Figure 4. PSD at 1700 s (with desorption).

Figures 6 and 7 show the flow rate of surfactant used in the simulations and the resultant concentration of micelles when desorption is neglected or included in the model, respectively. It can be seen that the same flow rate of surfactant does not give the same evolution of the concentration of micelles in both cases. Under desorption, the concentration of radicals in the aqueous phase is higher and therefore the nucleation rate is higher. The total number of particles produced is therefore smaller without desorption than with desorption (see Figures 8 and 9).

Observer Design

A continuous stream information about the evolution of the PSD is necessary for process control. However, the PSD is difficult to measure on-line and the process model involves a number of parameters that are sensitive to impurities and are difficult to identify. This necessitates the construction of an observer to monitor the PSD.

An observer combines the process model describing the chemical reactions and physical behavior with the existing on-line measurements to estimate the unknown parameters or states of the system on-line. Among these algorithms, the Kalman filter is often proposed in the literature. This filter requires solving the dynamic Riccati equation, which is nonlinear. For a system of dimension k, the dimension of the space of the Riccati equations is $(k^2 + k)/2$. Moreover, the choice of the weighting matrices of the Riccati equations is difficult. Therefore, the Kalaman filter becomes difficult to adjust and is time consuming.

Our approach consists in designing an observer that derives from the high-gain techniques (see, for instance, Bornard and Hammouri[24]; Deza et al.[25]; Gauthier et al.[26]; Gauthier and Kupka[27]; Farza et al.[28]; Hammouri et al.[29]; and Edouard et al.[30]). The gain of the proposed observer does not require solving any differential equation and its tuning is easier.

In the following, two estimators are constructed. The first one allows the estimation of the number of moles of radicals in the particles (μ) from the measured overall conversion. Then this estimate is used in a second observer to estimate the PSD assuming first a known model of $\bar{n}(r, t)$ and then with errors in the model of $\bar{n}(r, t)$, which is more usual.

Estimation of μ

Excitement of equation system 31 is attributed to particle formation either by micellar or homogeneous nucleations $[\Re_{nuc}(t)]$. The rate of nucleation is directly related to the concentrations of monomer $([M]_P^{sat})$, radicals $([IM_i^{\cdot}]$ for $z \leq i \leq j_{crit} - 1)$ and micelles $([Micelle])$ in the aqueous phase. However, the concentrations of radicals in the aqueous phase is sensitive to impurities and inhibitors and the concentration of micelles depends on a number of coefficients that are not well known (adsorption and desorption). This makes the process irreproducible and necessitates on-line measurement of the reaction rate and the kinetics in the aqueous phase.

In this work, the monomer conversion

$$X(t) = 1 - \frac{N_m(t)}{N_m(0)}$$

is assumed to be measured on-line. This can be done by calorimetry,[31-33] on-line gas chromatography, or by spectroscopy.

Based on this measurement, Othman et al.[34] developed an estimator of the parameter μ. The estimation of μ allows detection of inhibition and determination of the real value of the reaction rate. The estimation is based on the material balance of monomer given by Eq. 14. In this nonlinear equation, the sole unknown parameter is μ. This is similar to saying, μ is observable from the model 14 if the residual number of moles of monomer is measured. A high-gain nonlinear estimator could therefore be constructed to monitor μ:

$$\begin{cases} \dfrac{dN_m(t)}{dt} = Q_m - k_p\mu(t)[M]_P - 2\theta(\hat{N}_m - N_m) \\ \dfrac{d\mu(t)}{dt} = \dfrac{\theta^2}{k_p[M]_P}(\hat{N}_m - N_m) \end{cases} \tag{32}$$

where θ is a positive tuning parameter of the observer.

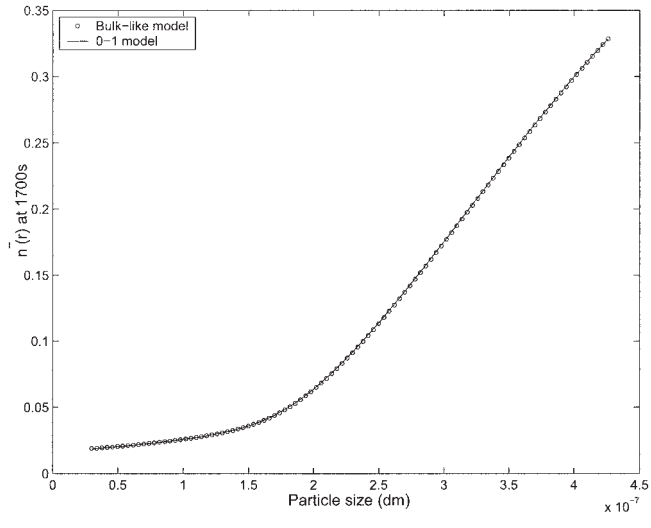

Figure 5. Average number of radicals per particle at 1700 s (with desorption).

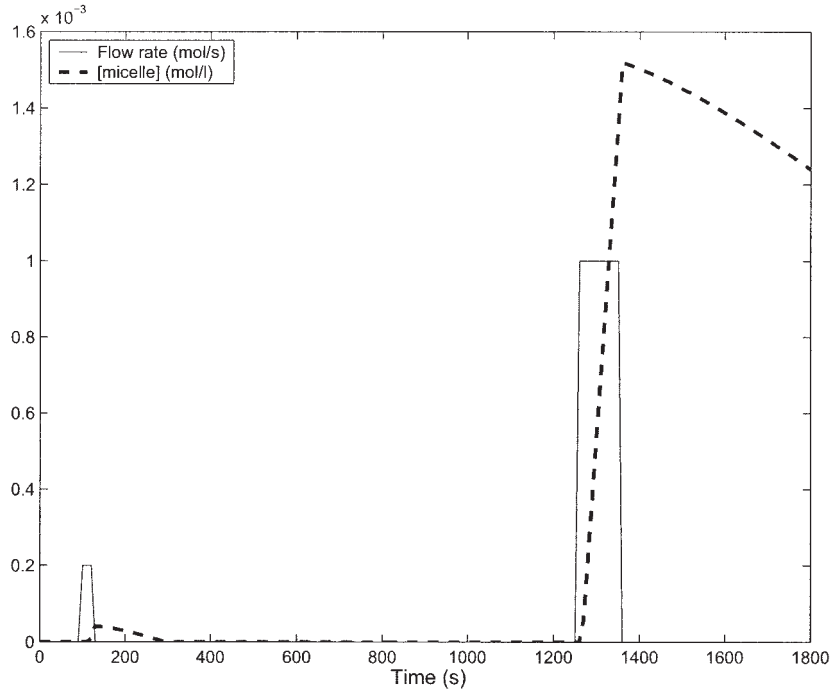

Figure 6. Surfactant flow rate and concentration of micelles (without desorption).

The PSD and the average number of radicals per particle will be estimated using the bulk-like model and based on the estimate of μ. The parameter μ contains information about the particles' number and the average number of radicals per particle. However, the PSD and the average number of radicals per particle are not observable using the unique information of μ.

To dissociate the influence of the PSD and the average number per particle on μ a model of $\bar{n}(r, t)$ will be used. If this model is very well known, then $\bar{n}(r, t)$ can be simulated in an open-loop manner and, in this case, $n(r, t)$ becomes observable because the unique unknown parameter. However, the known models of $\bar{n}(r, t)$ involve the kinetics in the aqueous phase that are not always reproducible, and the

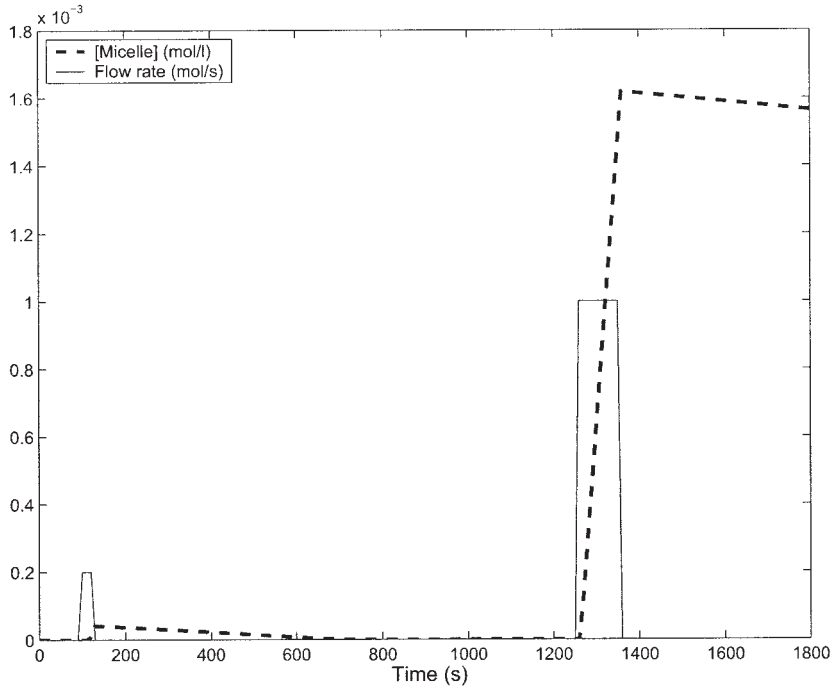

Figure 7. Surfactant flow rate and concentration of micelles (with desorption).

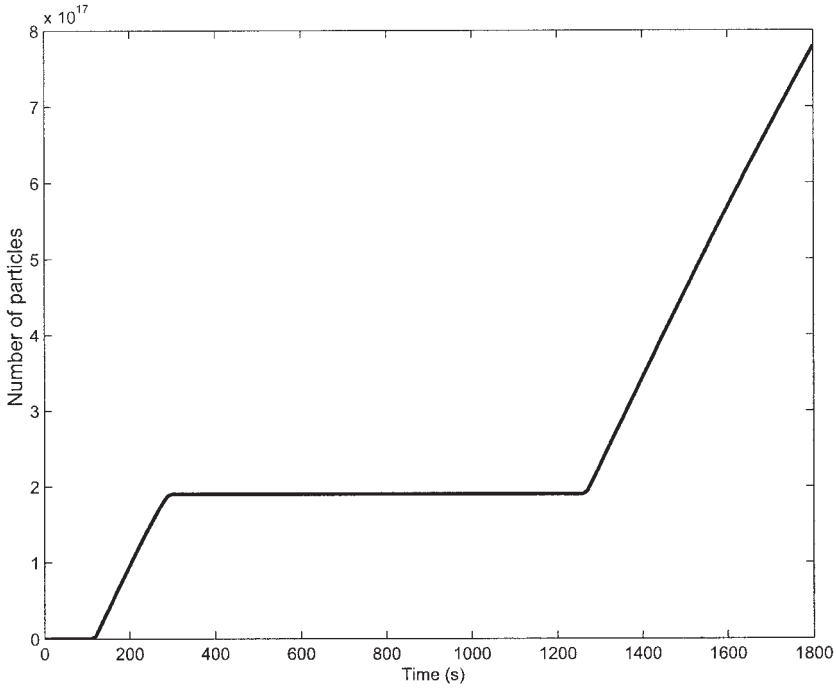

Figure 8. Total number of particles (without desorption).

parameters of absorption and desorption that might contain some irreproducibility. The model of $\bar{n}(r, t)$ must thus be adjusted on-line. This requires the use of a new measurement that decouples $\bar{n}(r, t)$ and $n(r, t)$. In this case, the average number of particles is supposed to be measured from time to time. This ensures the correction of the model of $\bar{n}(r, t)$ and thus allows estimation of the PSD.

Both cases will be studied in the following sections:

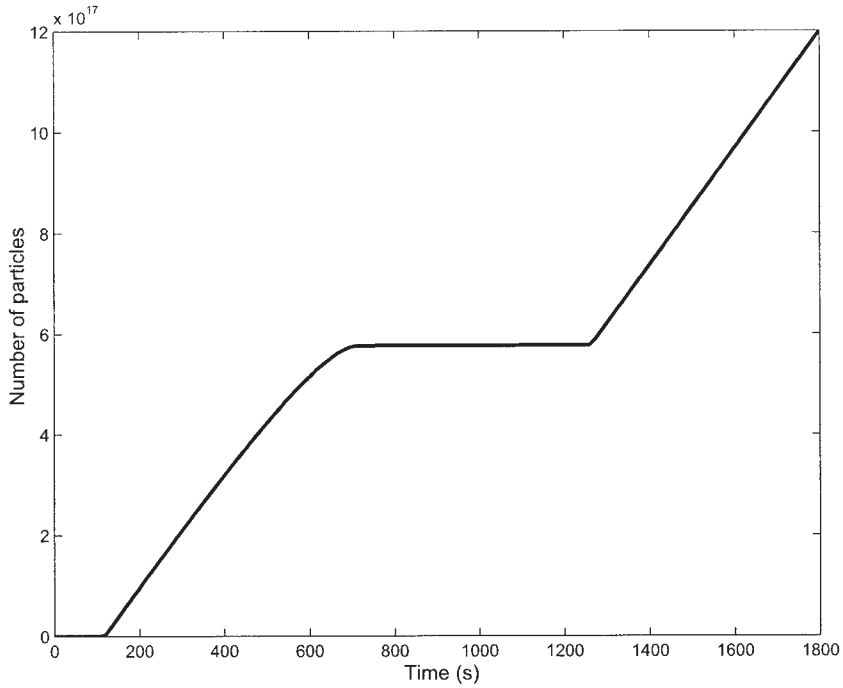

Figure 9. Total number of particles (with desorption).

- First, the model of $\bar{n}(r, t)$ is considered known.
- Second, uncertainties are considered in the model of $\bar{n}(r, t)$.

Estimation of the PSD with a well-known model of $\bar{n}(r, t)$

To estimate the nucleation rate and the PSD, the bulk-like model developed for the 0–1 system is used with the on-line measurement of the monomer conversion and the estimator of μ.

If μ is estimated on-line and if the model of $\bar{n}(r, t)$ is assumed to be accurate, then the dynamic of $N_p^T(t)$ can be estimated from the value of $\mu(t)$. Deriving Eq. 17 with respect to time, and using Eq. 31 gives the following expression:

$$\frac{dN_p^T(t)}{dt} = \frac{d}{dt}\int_{r_{nuc}}^{\infty} n(r, t)dr = G(r_{nuc})\bar{n}(r_{nuc}, t)n(r_{nuc}, t) = \Re_{nuc}(t) + G(r_\infty)\bar{n}(r_\infty, t)n(r_\infty, t) \quad (33)$$

However, if the domain of r is large enough such that the particles' size does not exceed it, then the following assumption can be made:

$$G(r_\infty)\bar{n}(r_\infty, t)n(r_\infty, t) = 0$$

Numerically, if the finite-elements method is used to solve the PSD, then this assumption can be ensured by using a high final particle size or by using a moving horizon of finite elements that is always higher than the largest particles.

This gives

$$\frac{dN_p^T(t)}{dt} = \Re_{nuc}(t) \quad (34)$$

Equation 34 shows that the nucleation rate is observable from the measurement of $N_p^T(t)$ that can be obtained from μ if $\bar{n}(t)$ is obtained by open-loop simulation. Because the nucleation rate is the sole parameter affecting the PSD, then the PSD can be reconstructed using the estimated value of $\Re_{nuc}(t)$ and Eq. 31a. This assumes that the kinetics of growth are well identified. In the case of well-known kinetics of coagulation, the estimation of the PSD based on the estimated rate of nucleation would also be possible using the same observer. Actually, the rate of coagulation is added to the rate of nucleation but with some dependency on the PSD. This would not affect the observability of the system. The nucleation rate remains observable from Eq. 33 where the known coagulation term is added.

The global extended model needed to construct the observer takes the following form:

$$\begin{cases} \dot{x}(t) = A(r)x(t) \\ y(t) = Cx(t) = [0\cdots 0100]x(t) = \dfrac{\mu(t) \times N_A}{\bar{n}(t)} = N_P^T(t) \end{cases} \quad (35)$$

where $x(t)$ is the state of the system of dimension $k + 3$, where k corresponds to the size of the finite-element approximation:

$$x(t) = \begin{pmatrix} x_1(t) \\ \vdots \\ x_k(t) \\ x_{k+1}(t) \\ x_{k+2}(t) \\ x_{k+3}(t) \end{pmatrix} = \begin{pmatrix} n(r_{nuc} + k\delta r, t) \\ \vdots \\ n(r_{nuc} + \delta r, t) \\ N_p^T(t) \\ \Re_{nuc}(t) \\ \varepsilon(t) \end{pmatrix}$$

Note that, the unknown dynamic of $\Re_{nuc}(t)$ is represented by $\varepsilon(t)$, and $A(r)$ is given by

$$A(r) = \begin{pmatrix} -a_k & a_{k-1} & 0 & \cdots & \cdots & 0 & 0 \\ 0 & -a_{k-1} & a_{k-2} & 0 & \cdots & \cdots & 0 \\ \vdots & 0 & \ddots & \ddots & \ddots & \cdots & 0 \\ 0 & \cdots & 0 & -a_1 & 0 & 1 & 0 \\ 0 & \cdots & \cdots & 0 & 0 & 1 & 0 \\ 0 & \cdots & \cdots & \cdots & \cdots & 0 & 1 \\ 0 & \cdots & \cdots & \cdots & \cdots & \cdots & 0 \end{pmatrix}$$

The a_i expressions are given by the following equation:

$$a_i = G(r_{nuc} + i\delta r)\bar{n}(r_{nuc} + i\delta r, t)/\delta r \quad (36)$$

The dynamic structure of Eq. 35 is under a canonical form of observability, which allows us to construct a high-gain observer (see, for example, Farza et al.[35]) as given by the following system:

$$\begin{cases} \dot{\hat{x}}(t) = A(r)\hat{x}(t) - \Theta[\hat{x}_{k+1}(t) - y(t)] \\ y(t) = \dfrac{\mu(t) \times N_A}{\bar{n}(t)} \end{cases} \quad (37)$$

where

$$\Theta = \begin{pmatrix} 0 \\ \vdots \\ 0 \\ 3\theta \\ 5\theta^3 \\ \theta^5 \end{pmatrix}$$

The positive parameter θ allows us to adjust the observer convergence rate. Using a high value of θ allows the observer to converge quickly to the set point but amplifies measurement noise. In our case, the best value obtained by simulation corresponds to $\theta = 7$. It can be seen that the first k states, representing the PSD, do not have a corrective term. In fact, the observer allows us to filter $N_p^T(t)$ and gives an estimate of the nucleation rate $r_{nuc}(t)$. The nucleation rate is then introduced in Eq. 31 to calculate the entire PSD.

Figure 10 gives the surfactant feed rate used in the simulation. The resulting free surfactant concentration resulting from the addition of surfactant is presented in Figure 11. The estimation results using equation system 35 combined with Eq. 31b are shown in Figures 12 to 14. It can be seen that the estimator converges well to the process model. Figure 12 shows that the

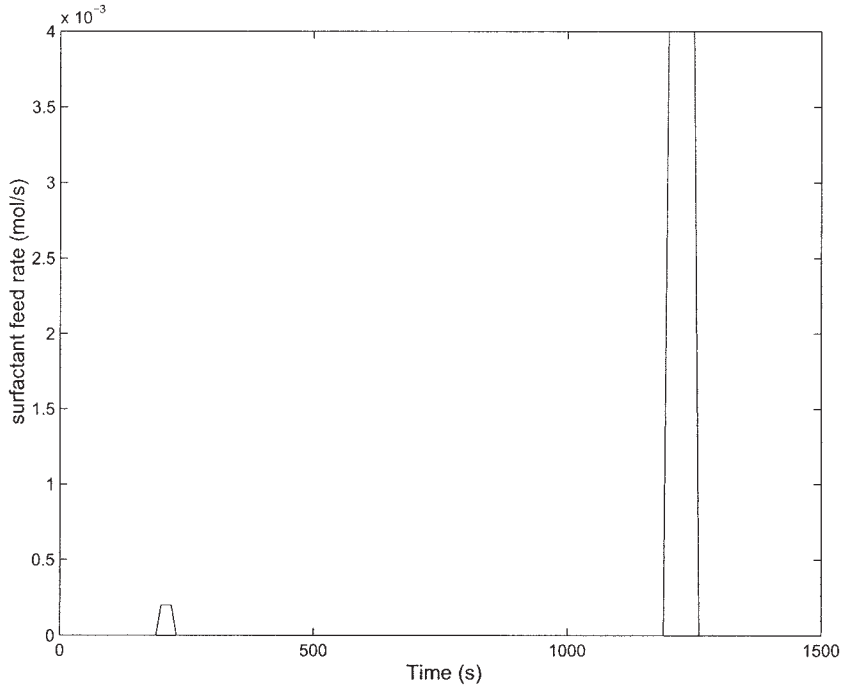

Figure 10. Feed rate of surfactant.

nucleation rate increases when the concentration of surfactant exceeds the CMC, which results in two nucleation times. The second time is saturated by the concentration of radicals present in the aqueous phase. Figure 13 shows that the average number of radicals per particle is 0.5 during homogeneous nucleation and then decreases to 0.1 during micellar nucleation and is maintained very small during the growth of particles. Finally, the PSD at 1500 s is shown in Figure 14. The estimator reconstructs the estimation of the PSD very well.

The observer developed in this section thus allows us to estimate the PSD from the measurement of the monomer conversion even under disturbances if the model of $\bar{n}(r, t)$ is supposed to be accurate. However, the model of $\bar{n}(r, t)$ contains uncertainties arising from inhibition and possible errors of parameter estimation. For this reason, the observer must be adapted in a way that allows the estimation of the PSD even under uncertainties in the model of $\bar{n}(r, t)$. Figures 15 and 16 show the influence of $\bar{n}(r, t)$ on the PSD. Actually, $\bar{n}(r, t)$ and therefore $\bar{n}(t)$ have a direct influence

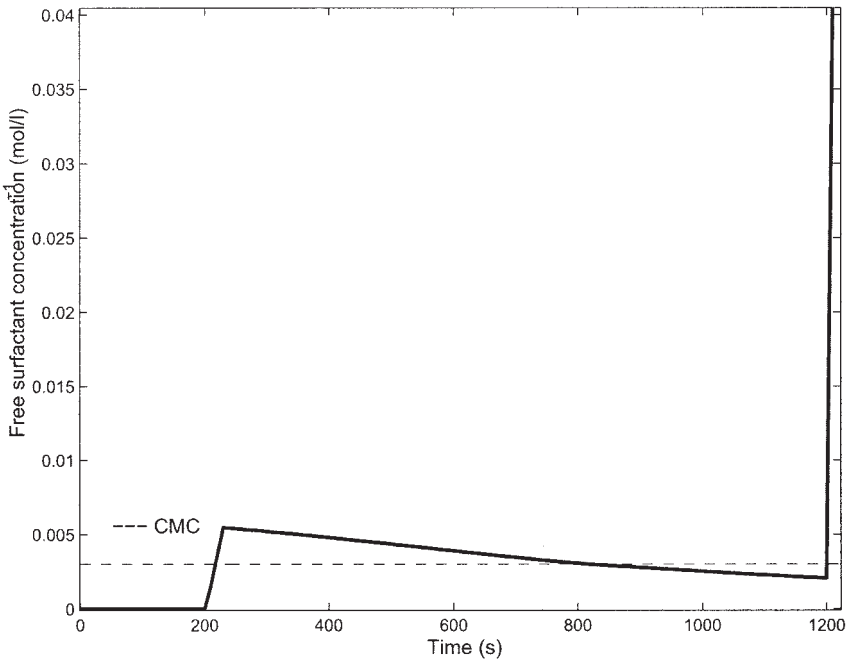

Figure 11. Concentration of free surfactant.

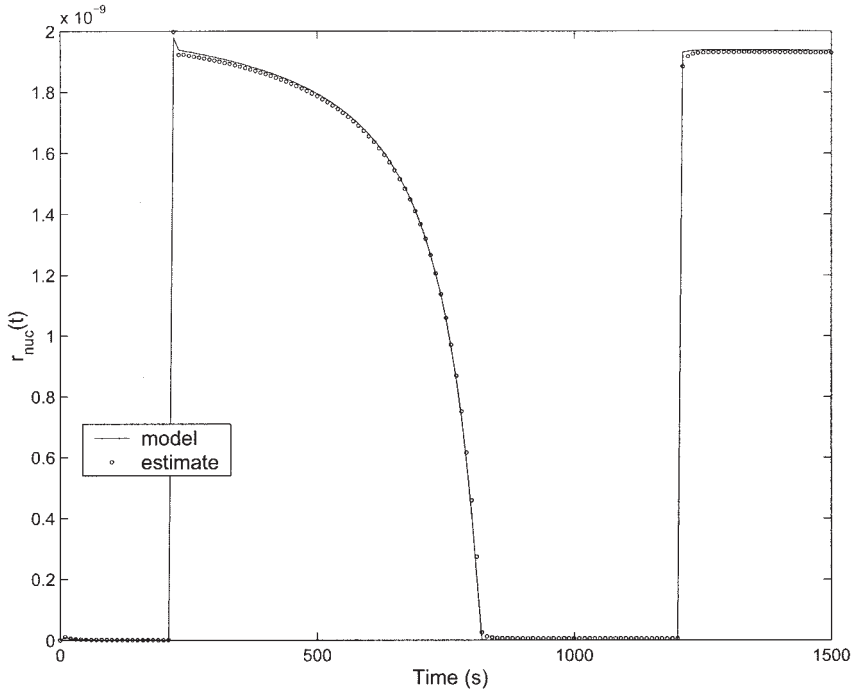

Figure 12. Estimation of the nucleation rate.

on the nucleation rate and on the rate of polymerization by influencing the parameter $\mu(t)$ in Eq. 16. To illustrate this importance, simulation of the PSD was done with a constant value of $\bar{n}(r, t)$. These results were then compared to the simulation using the value of $\bar{n}(r, t)$ obtained from the equation model 31a. The two following values were used in the simulations and are called "estimate (1)" and "estimate (2)," whereas the real value obtained from the model is called "model":

Estimate (1)

$$\bar{n}(r) = \begin{pmatrix} 0.2 \\ \vdots \\ 0.2 \end{pmatrix}$$

and thus $\bar{n} = 0.2$.

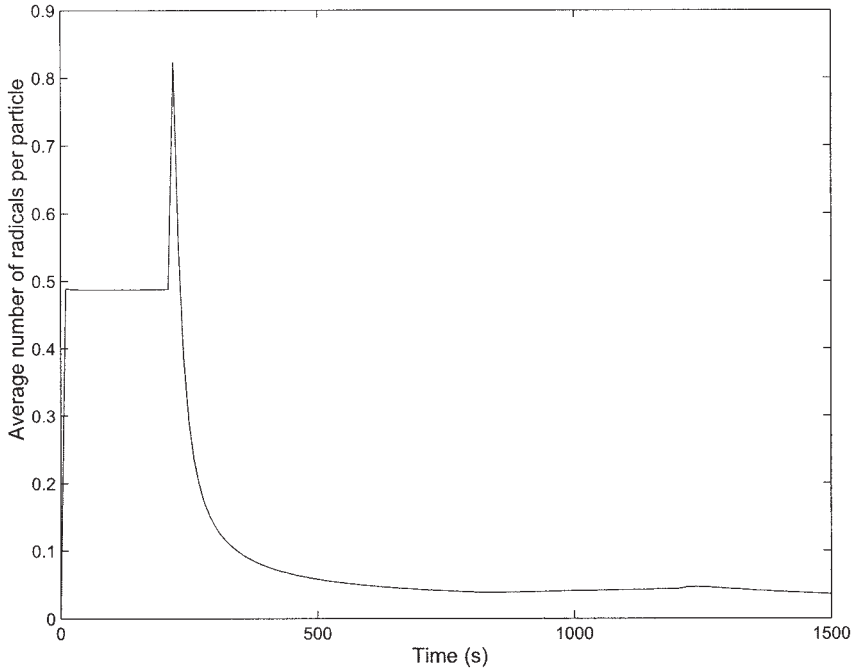

Figure 13. Estimation of $\bar{n}(t)$.

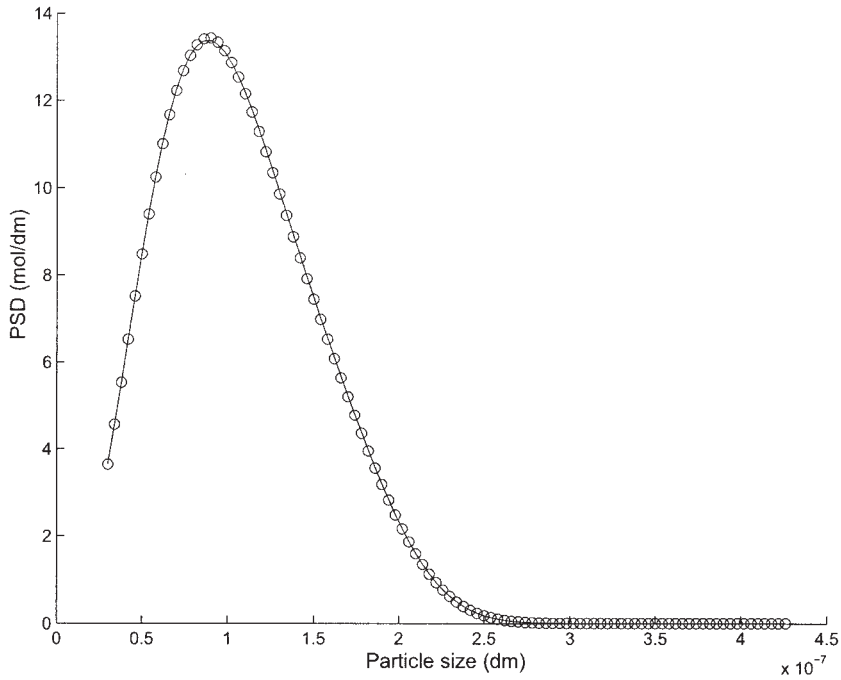

Figure 14. Estimated PSD at 1500 s.

Estimate (2)

$$\bar{n}(r) = \begin{pmatrix} 1 \\ \vdots \\ 1 \end{pmatrix}$$

and thus $\bar{n} = 1$.

Figure 15 shows that $\bar{n}(r, t)$ substantially affects the nucleation rate and therefore the PSD. Figures 16a, 16b, and 16c represent the real PSD and the PSD obtained by the constant values of $\bar{n}(r, t)$, "estimate (1)" and "estimate (2)," respectively. This shows that in-depth knowledge of $\bar{n}(r, t)$ is necessary to obtain the real PSD. The open-loop simulation of the model of $\bar{n}(r, t)$ that might undergo uncertainties is not effi-

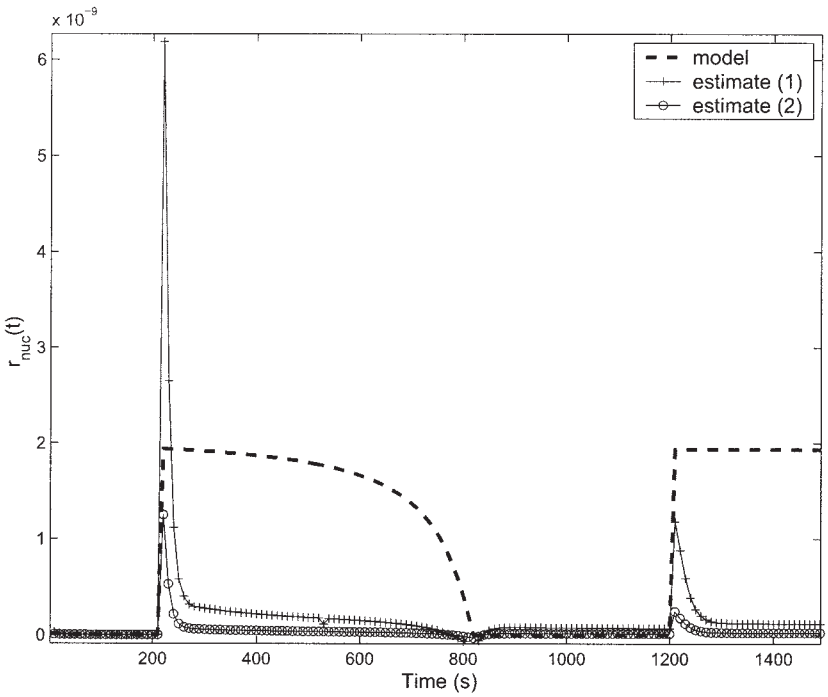

Figure 15. Influence of the value of $\bar{n}(r, t)$ on the nucleation rate.

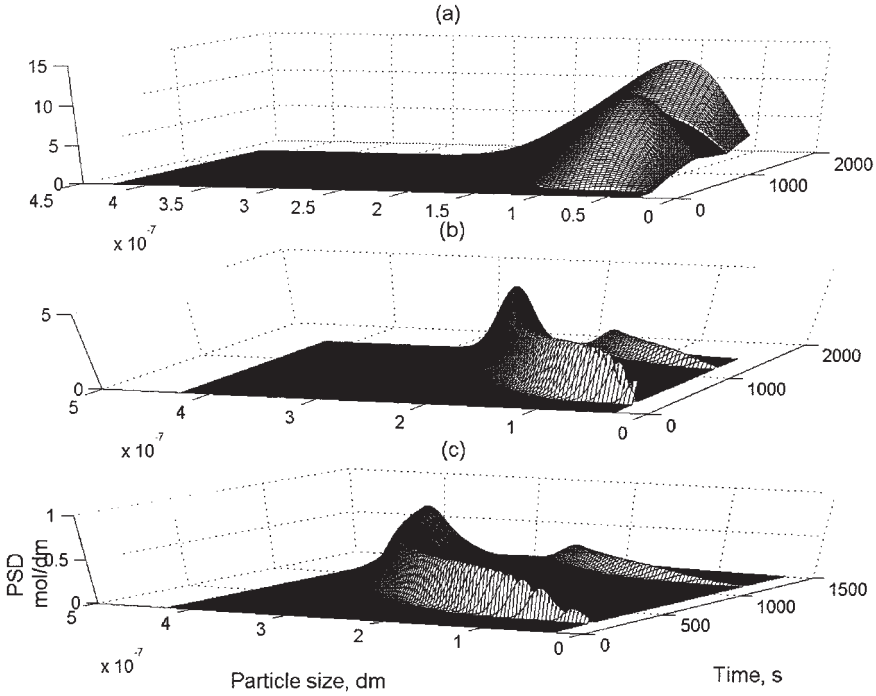

Figure 16. Influence of the value of $\bar{n}(r, t)$ on the PSD.

cient. In the following section, an observer is developed to take into account any uncertainties in the model of $\bar{n}(r, t)$.

Estimation of the PSD assuming uncertainties on the model of $\bar{n}$ (r, t)

To estimate $n(r, t)$ and $\bar{n}(r, t)$ simultaneously, the observer should be able to overcome inaccuracies in the model used for the estimation, especially concerning the model of $\bar{n}(r, t)$ that is sensitive to impurities.

If the model of $\bar{n}(r, t)$ undergoes any uncertainties, then it cannot be used in an open-loop manner to estimate the PSD. The unique measurement of the monomer conversion does not permit one to update the model of $\bar{n}(r, t)$ and to estimate $N_p^T(t)$. To take into account uncertainties in the model of $\bar{n}(r, t)$, a new measurement has to be done to distinguish the influence of $\bar{n}(t)$ and $N_p^T(t)$ on the parameter $\mu(t)$.

This can be done either by measuring $\bar{n}(r, t)$ or $n(r, t)$ at discrete intervals, which allows one to update the model of $\bar{n}(r, t)$. However, a discrete measurement of the PSD is not usually available and requires sophisticated apparatus such as CHDF. Nevertheless, to decouple the influence of $\bar{n}(t)$ and $N_p^T(t)$ on the parameter $\mu(t)$, measuring $\bar{n}(t)$ or $N_p^T(t)$ at discrete intervals might be sufficient. This would allow to update the model of $\bar{n}(r, t)$. Experimentally, the average size of particles can be measured easily and quickly by light scattering, which allows us to calculate $N_p^T(t)$.

The monitoring strategy thus consists of measuring the monomer conversion continuously and measuring the average particle size (therefore the total number of particles) at discrete intervals. Based on the monomer conversion measurement, the parameter μ is estimated using the observer presented by equation system 32. The PSD observer (Eq. 37) is then applied to estimate the PSD using a simplified model of $\bar{n}(r, t)$, which is derived from Eq. 31a by maintaining the most important terms numerically.

Let us consider Eq. 31a again:

$$\frac{\partial \bar{n}(r, t)}{\partial t} = \underbrace{\rho(r, t)[1 - 2\bar{n}(r, t)]}_{A(r,t)} + \frac{\partial G(r)\bar{n}(r, t)n(r, t)}{\partial r}\left[\frac{\bar{n}(r, t) - 1}{n(r, t)}\right] + \underbrace{k_{des}(r)\left\{\frac{\rho_{ent-m}(r, t)[\bar{n}(r, t) - 1]}{\rho(r, t) + [M]_P(k_{pe} + k_{tr}) + k_{des}(r)} - \frac{k_{tr}[M]_P\bar{n}(r, t)}{\rho(r, t) + [M]_P(k_{pe} + k_{tr}) + k_{des}(r)}\right\}}_{B(r, t)} \quad (38)$$

In this equation, $A(r, t)$ and $B(r, t)$ are functions of the concentration of radicals in the aqueous phase (IM_3 and IM_4) and the concentration of micelles ([*Micelle*]). To calculate these terms exactly, the desorption and adsorption phenomena should be accounted for. These terms thus imply an important calculation time. However, a rapid numerical analysis of these

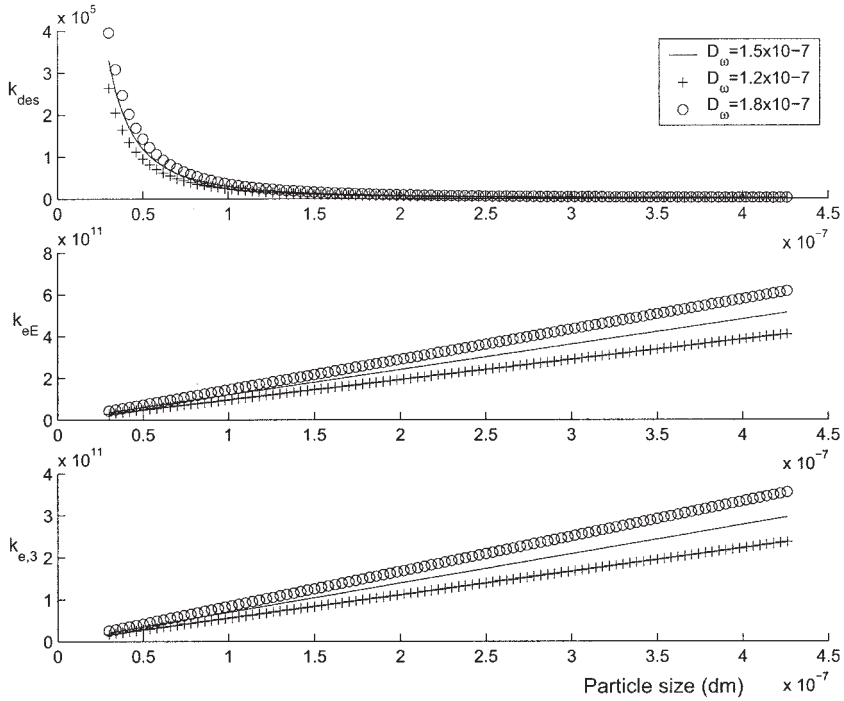

Figure 17. Influence of the parameter D_w on the parameters k_{des}, k_{eE}, and $k_{e,3}$.

terms showed that the terms $A(r, t)$ and $B(r, t)$ have a slow dynamic and do not change abruptly even under nucleation. The second term is the most sensitive to nucleation and undergoes a rapid dynamic. This allows us to neglect changes coming from the terms $A(r, t)$ and $B(r, t)$ if they are well initialized. In this way, we ensure that we take into account any nucleation that would guarantee having the good PSD by the continuous observer presented in the previous section.

The following model of $\bar{n}(r, t)$ can therefore be derived from Eq. 38:

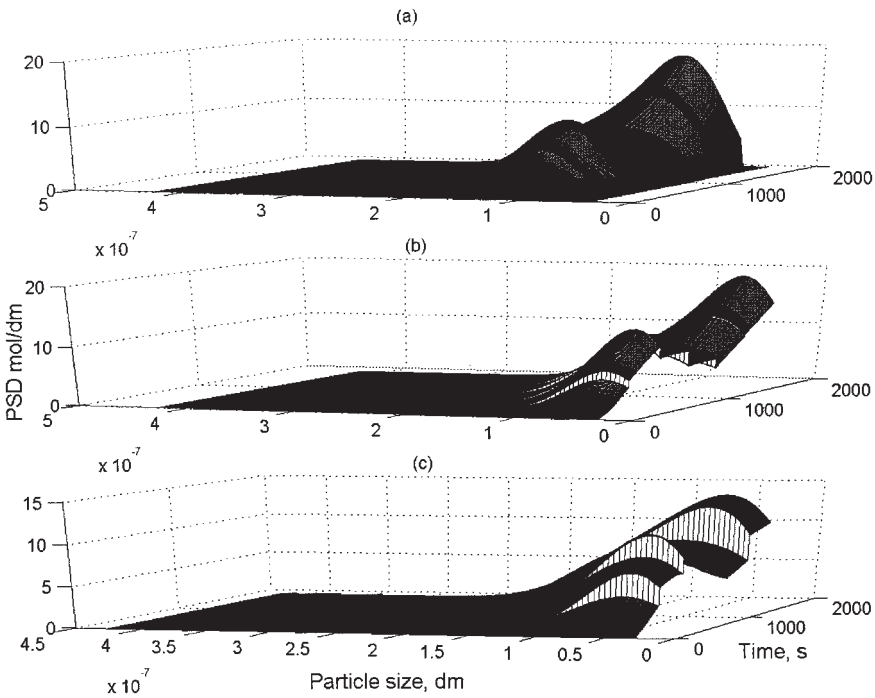

Figure 18. Estimation of the PSD by the continuous-discrete observer.

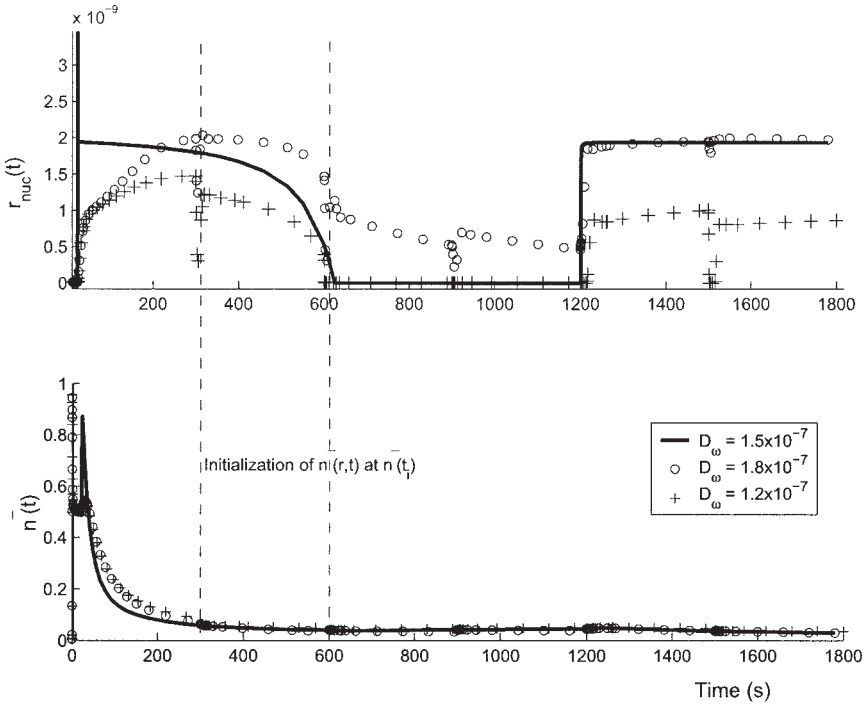

Figure 19. Estimation of the nucleation rate by the continuous-discrete observer.

$$\frac{\partial \bar{n}(r,\,t)}{\partial t} = \frac{\partial G(r)\bar{n}(r,\,t)n(r,\,t)}{\partial r}\left[\frac{\bar{n}(r,\,t)-1}{n(r,\,t)}\right] \qquad (39)$$

Initialization of this equation becomes the crucial step of the estimation. Using the discrete measurement of N_p^T, $\bar{n}(t)$ is estimated and the model of $\bar{n}(r, t)$ (Eq. 39) is reinitialized at this estimated value.

The estimation results are presented in Figures 17–19. Error in the model of $\bar{n}(r, t)$ was mainly supposed to become from the rate of diffusion (D_w) that is supposed to influence the rate of absorption of monomeric radicals (k_{eE}) and the rate of desorption (k_{des}). Figure 17 presents the influence of the parameter D_w on the parameters k_{des}, k_{eE}, and $k_{e,3}$. It can be seen that D_w primarily influences the parameter k_{eE}.

Figure 18 presents the estimation of the PSD using the

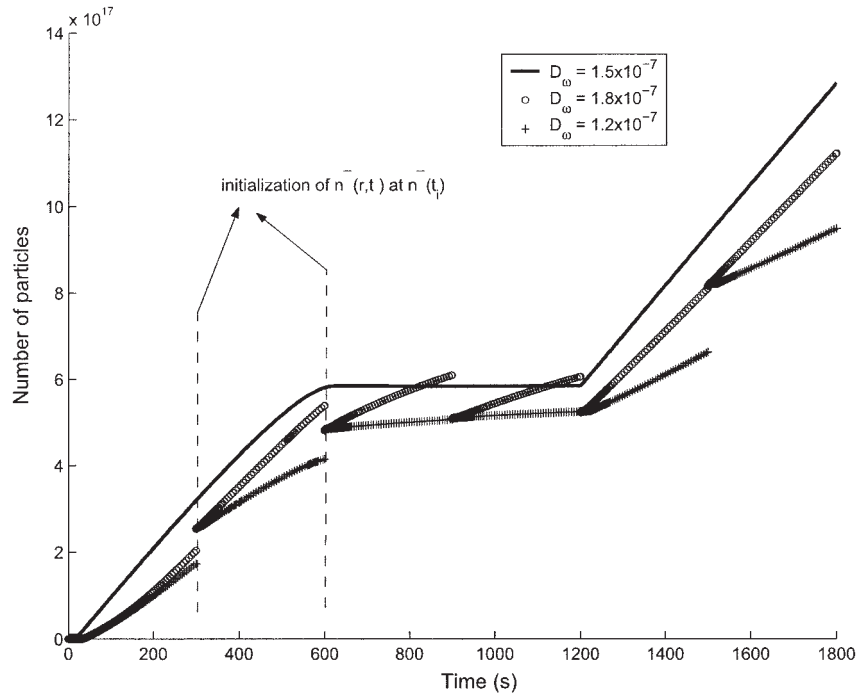

Figure 20. Estimation of the particles' number by the continuous-discrete observer.

continuous-discrete observer. Figure 18a represents the real PSD ($D_w = 1.5 \times 10^{-7}$). Figures 18b and 18c represent the estimated PSD with an error on D_w ($D_w = 1.2 \times 10^{-7}$ and $D_w = 1.8 \times 10^{-7}$) with a discrete correction every 300 s. In the second part of the figure, it can be seen that $\bar{n}(t)$ is well estimated. An error of estimation can be seen on the estimation of the nucleation rate, presented in the first part of Figure 19. However, it can be observed that both populations could be detected. This is because the nucleation could be detected by the growth term in Eq. 38. This is shown in Figure 19 representing the estimation of the nucleation rate and $\bar{n}(t)$. As in the previous figures, $D_w = 1.5 \times 10^{-7}$ represents the real process and the other curves correspond to the observer with an error on D_w. It can be seen that these curves tend to converge to the real process at each correction (every 300 s) and then return quickly to the normal model dynamic, although these corrections ensure the best detection of nucleation.

Corrections can also be seen in Figure 20, representing the estimation of the number of particles by the continuous-discrete observer. At each step of correction, a jump of the estimated curve of N_P^T is remarked, which allows us to stay close to the real PSD. The rate of change in the number of particles is detected in both cases ($D_w = 1.2 \times 10^{-7}$ and $D_w = 1.8 \times 10^{-7}$). The estimated number of particles increases at the middle, although no nucleation is taking place. This arises from the error in estimating the nucleation rate. However, the rate of increase is smaller than that detected during nucleation.

It is worthy noting, however, that these corrections can be ameliorated if the real PSD is measured from time to time, rather than an average diameter value. Even without any supplementary measurements, this method can be used for feedback control of the PSD. Actually, nucleation could be detected and therefore the entire PSD could be reconstructed based on this estimate.

Conclusions

In this work, a new bulk-like model was developed to represent the PSD in the 0–1 system. The new model is easier to handle and makes possible the continuity between the 0–1 system (small particles) and the pseudobulk system (large particles).

Based on this new model, a continuous-discrete observer was developed to estimate the PSD and the average number of radicals per particle simultaneously.

The observer is able to undergo modeling errors. An error was supposed in the rate of desorption and absorption of radicals, although the observer was able to detect nucleation and to reconstruct the PSD.

This strategy should be a good tool for the control of the PSD. Actually, the observer can be included in a control scheme to manipulate the control variables: surfactant or initiator flow rates to obtain a target PSD.

Notation

a_{sd} = surface area of droplets covered by a single surfactant molecule (4.2×10^{-17}), dm^2
a_{sp} = surface area of particles covered by a single surfactant molecule (4.2×10^{-17}), dm^2
b_s = Langmuir adsorption isotherm parameter (related to the surfactant coverage area ratio) (2.1×10^3), dm^3/mol
CMC = critical micellar concentration (3×10^{-3}), mol/dm^3
d_m = monomer density (0.878), kg/dm^3
d_p = polymer density (1.044), kg/dm^3
D_w = diffusion coefficient for monomer in water (1.5×10^{-7}), dm^2/s
$[E]$ = concentration of monomeric radicals, mol/dm^3
$G(r)$ = particle growth, dm/s
$[IM_i]$ = aqueous phase concentration of oligomeric radicals of degree i, mol/dm^3
$[I]$ = concentration of primary initiated radicals, mol/dm^3
j_{crit} = chain length at which the radicals become insoluble in water and principate (5)
K_{d-aq} = coefficient of monomer partitioning between monomer droplets and the aqueous phase (1966)
K_{p-aq} = coefficient of monomer partitioning between polymer particles and the aqueous phase ($[M]_{aq}^{sat}/[M]_P^{sat} = 1348$)
k_d = coefficient of initiator decomposition rate (7.4×10^{-7}), s^{-1}
$k_{em,i}$ = coefficient of the rate of radical entry into micelles, $dm^3\ mol^{-1}\ s^{-1}$
$k_{e,i}$ = coefficient of the rate of radical entry into particles of size r, $dm^3\ mol^{-1}\ s^{-1}$
k_{eE} = coefficient of the rate of entry of monomeric radicals into particles of size r, $dm^3\ mol^{-1}\ s^{-1}$
k_{des} = coefficient of the desorption rate of monomeric radicals, s^{-1}
k_p = coefficient of monomer propagation into particles (260), $dm^3\ mol^{-1}\ s^{-1}$
k_{pI}^{aq} = coefficient of initiation rate ($=100 \times k_p$), $dm^3\ mol^{-1}\ s^{-1}$
$k_{p,1}^{aq}$ = coefficient of propagation of monomer with a one-unit radical (1200), $dm^3\ mol^{-1}\ s^{-1}$
$k_{p,2}^{aq}$ = coefficient of propagation of monomer with a two-unit radical (280), $dm^3\ mol^{-1}\ s^{-1}$
$k_{p,i}^{aq}$ = coefficient of propagation of monomer with an i-unit radical ($i = 3, 4$) ($=k_p$), $dm^3\ mol^{-1}\ s^{-1}$
k_{pe} = coefficient of propagation of monomeric radicals (260), $dm^3\ mol^{-1}\ s^{-1}$
k_t^{aq} = coefficient of termination in the aqueous phase (1.16×10^9), $dm^3\ mol^{-1}\ s^{-1}$
k_{tr} = coefficient of transfer to monomer in the polymer particles (9.3×10^{-3}), $dm^3\ mol^{-1}\ s^{-1}$
k_{tr}^{aq} = coefficient of transfer to monomer in the aqueous phase ($=k_{tr}$), $dm^3\ mol^{-1}\ s^{-1}$
$[M]_{aq}$ = concentration of monomer in the aqueous phase, mol/dm^3
$[M]_{aq}^{sat}$ = concentration of monomer in the aqueous phase under saturation, mol/dm^3
$[M]_P$ = concentration of monomer in the polymer particles, mol/dm^3
$[M]_P^{sat}$ = concentration of monomer in the polymer particles under saturation, mol/dm^3
$[Micelle]$ = concentration of micelles, mol/dm^3
m_p = polymer mass, kg
MW_m = monomer molecular weight (0.104), kg/mol
$N(r, t)$ = total number of particles
N_A = Avogadro's number, mol^{-1}
N_m = number of moles of free monomer in the reactor, mol
N_S = total number of moles of surfactant in the reactor, mol
N_S^P = number of moles of surfactant adsorbed on the surface of particles, mol
N_S^d = number of moles of surfactant adsorbed on the monomer droplets, mol
N_S^{aq} = number of moles of surfactant in the aqueous phase, mol
$n(r, t)$ = number of moles of particles of size between r and $r + dr$ at time t, mol
$n_{0(r,}\ t)$ = number of moles of particles of size between r and $r + dr$ containing no radicals at time t, mol
$n_{1m}(r, t)$ = number of moles of particles of size between r and $r + dr$ containing a monomeric radical at time t, mol
$n_{1p}(r, t)$ = number of moles of particles of size between r and $r + dr$ containing a polymeric radical at time t, mol
n_{agg} = micellar aggregation number (average number of surfactant molecules in micelles) (60)
$\bar{n}(r, t)$ = average number of radicals in particles of size r at time t
$\bar{n}(t)$ = average number of radicals in the polymer particles of any size at time t
Q_I = flow rate of initiator, mol/s
Q_m = flow rate of monomer, mol/s
r_{mic} = radius of micelles (2.6×10^{-8}), dm

r_{nuc} = nucleation radius ($=r_{mic}$), dm
r_d = radius of the monomer droplets (1×10^{-4}), dm
r_s = swollen radius, dm
R_P = polymerization rate, mol/s
$\Re_{nuc}$ = nucleation rate, mol/s
$\Re_{nuc-hom}$ = rate of homogeneous nucleation, mol/s
$\Re_{nuc-mic}$ = rate of micellar nucleation, mol/s
$[S^{aq}]$ = concentration of surfactant in the aqueous phase, mol/dm^3
S_{par} = total particle surface, dm^2
$[T]$ = total concentration of radicals in the aqueous phase, mol/dm^3
V^{aq} = aqueous phase volume, dm^3
V^d = volume of the monomer droplets, dm^3
z = critical chain length at which polymer radicals can enter polymer particles or micelles causing micellar nucleation (3)
μ = number of moles of radicals in the polymer particles, mol
$\rho(r, t)$ = overall rate of radical entry into particles, mol/s
$\rho_{ent-r}(r, t)$ = rate of entry of a radical of length i ($z \leq i \leq j_{crit-1}$) into particles, mol/s
$\rho_{ent-m}(r, t)$ = rate of entry of a monomeric radical into particles, mol/s

Literature Cited

1. Geurts JM, Lammers M, German AL. The effect of bimodality of the particle size distribution on film formation of latices. *Colloids Surf A Physicochem Eng Aspects.* 1996;108:295-303.
2. Guyot A, Chu F, Schneider M, Graillat C, McKenna TF. High solid content latexes. *Prog Polym Sci.* 2002;27:1573-1615.
3. Santos AF, Lima EL, Pinto JC. In-line evaluation of average particle size in styrene suspension polymerizations using near-infrared spectroscopy. *J Appl Polym Sci.* 1998;70:1737-1745.
4. Immanuel ChD, Crowley TJ, Meadows ES, Cordeiro CF, Doyle FJ III. Evolution of multimodal particle size distribution in vinly acetate/butyl acrylate emulsion copolymeriztions. *J Polym Sci Part A: Polym Chem.* 2003;41:2332-2249.
5. Schneider M, Claverie J, Graillat C, McKenna TF. High solids content emulsions. I. A study of the influence of the particle size distribution and polymer concentration on viscosity. *J Appl Polym Sci.* 2002;84:1878-1896.
6. Bartsch S, Kuliche WM, Fresen I, Moritz U. Seeded emulsion polymerization of styrene: Determination of particle size by flow field-flow fractionation coupled with multi-angle laser light scattering. *Acta Polym.* 1999;50:373-380.
7. Gilbert RG. *Emulsion Polymerization, A Mechanistic Approach.* San Diego, CA: Academic Press; 1995.
8. Coen EM, Gilbert RG, Morrison BR, Leube H, Peach S. Modeling particle size distribution and secondary particle formation in emulsion polymerization. *Polymer.* 1998;39:7099.
9. Sood A. Particle size distribution control in emulsion polymerization. *J Appl Polym Sci.* 2004;92:2884-2902.
10. Immanuel ChD, Cordeiro CF, Sundaram SS, Meadows ES, Crowley TJ, Doyle FJ III. Modeling of particle size distribution in emulsion co-polymerization: Comparison with experimental data and parametric sensitivity studies. *Comput Chem Eng.* 2002;26:1133-1152.
11. Storti G, Carra S, Morbidelli M. Kinetics of multi monomer emulsion polymerization: The pseudo-homopolymerization approach. *J Appl Polym Sci.* 1989;37:2443-2467.
12. Ginsburger E, Pla F, Fonteix Ch. Modeling and simulation of batch and semi-batch emulsion copolymerization of styrene and butyl acrylate. *Chem Eng Sci.* 2003;58:4493-4514.
13. Ramkrishna D. *Population Balances: Theory and Applications to Particulate Systems in Engineering.* San Diego, CA: Academic Press; 2000.
14. Immanuel ChD, Doyle FJ III. Computationally efficient solution of population balance models incorporating nucleation growth and coagulation: Application to emulsion polymerization. *Chem Eng Sci.* 2003;58:3681-3698.
15. Semino D, Ray WH. Control of systems described by population balance equations—I. Controllability analysis. *Chem Eng Sci.* 1995;50:1805-1824.
16. Semino D, Ray WH. Control of systems described by population balance equations—II. Emulsion polymerization with constrained control action. *Chem Eng Sci.* 1995;50:1825-1839.
17. Ohmura N, Kataoka K, Watanabe Sh, Okubo M. Controlling particle size by self-sustained oscillations in continuous emulsion polymerization of vinyl acetate. *Chem Eng Sci.* 1998;53:2135.
18. Crowley T, Meadows ES, Kostoulas E, Doyle FJ III. Control of particle size distribution described by a population balance model of semibatch emulsion polymerization. *J Process Control.* 2000;10:419-432.
19. Zeaiter J, Romagnoli JA, Barton GW, Gomes VG, Hawkett BS, Gilbert RG. Operation of semi-batch emulsion polymerization reactors: Modeling, validation and effect of operating conditions. *Chem Eng Sci.* 2002;57:2955-2969.
20. Immanuel ChD, Doyle FJ III. Open-loop control of particle size distribution in semi-batch emulsion copolymerization using a genetic algorithm. *Chem Eng Sci.* 2002;57:4415-4427.
21. Immanuel ChD, Doyle FJ III. Hierarchical multiobjective strategy for particle-size distribution control. *AIChE J.* 2003;49:2383-2399.
22. Doyle FJ III, Harrison ChA, Crowley TJ. Hybrid model-based approach to batch-to-batch control of particle size distribution in emulsion polymerization. *Comput Chem Eng.* 2003;27:1153-1163.
23. Coen EM, Peach S, Morrison BR, Gilbert RG. First-principles calculation of particle formation in emulsion polymerization: Pseudo-bulk systems. *Polymer.* 2004;45:3595-3608.
24. Bornard G, Hammouri H. A high gain observer for a class of uniformly observable systems. Proc of the 30th IEEE Conference on Decision and Control, Brighton, UK; 1991:1494.
25. Deza F, Busvelle E, Gauthier JP. High gain estimation for nonlinear systems. *Syst Control Lett.* 1992;18:295.
26. Gauthier JP, Hammouri H, Othman S. A simple observer for nonlinear systems: Application to bioreactors. *IEEE Trans Autom Control.* 1992;37:875.
27. Gauthier JP, Kupka IAK. Observability and observers for nonlinear systems. *SIAM J Control Optim.* 1994;32:975.
28. Hammouri M, Farza H, Busavon K. A simple observer for a class of nonlinear systems. *Appl Mater Lett.* 1998;11:27.
29. Hammouri H, Targui B, Armanet F. High gain observer based on a triangular structure. *Int J Robust Nonlinear Control.* 2002;12:497.
30. Edouard D, Schweich D, Hammouri H. Observer design for reverse flow reactor. *AIChE J.* 2004;50:2155-2166.
31. Arzamendi G, Asua J. Copolymer composition control of emulsion copolymer in reactors with limited capacity for heat removal. *Ind Eng Chem.* 1991;30:1342-1350.

Manuscript received Jan. 5, 2005, and revision received Mar. 22, 2005.